Thermal encapsulation of large battery packs for electric vehicles operating in cold climate

Applied Thermal Engineering 212 (2022) 118548

Contents lists available at ScienceDirect

Applied Thermal Engineering

journal homepage: www.elsevier.com/locate/ate

Research Paper

Thermal encapsulation of large battery packs for electric vehicles operating in cold climate☆

Anandh Ramesh Babu [a,*], Blago Minovski [b], Simone Sebben [a]

[a] Division of Vehicle Engineering and Autonomous Systems, Chalmers University of Technology, Sweden
[b] Volvo Group Truck Technology, Sweden

ARTICLE INFO

Keywords:
Passive battery thermal management
Thermal insulation
Low-temperature performance
Lithium-ion battery
Electric vehicle

ABSTRACT

Thermal management for electric vehicles is becoming ever more significant for ensuring prolonged driving range. Climatization of batteries to the optimal operating temperatures is crucial for their performance and lifetime, and therefore they need to be heated when operating in cold climate. This often results in reduced driving range. This work numerically investigates the potential of thermal encapsulation of large battery packs for electric truck applications. Vehicle-level simulations were performed under drive cycle conditions at different operating temperatures to study its influence on the battery performance. Parking–driving cycles at various ambient temperatures and a parametric study on the encapsulation characteristics were carried out to assess the energy consumption under each condition. The study shows that high thermal resistance of the insulation material significantly reduced the heat loss to the environment acclimatizing the battery pack close to near-optimal operating temperatures, which can result in potential energy savings of about 15% at −25 °C when operating after a 12-h parking period.

1. Introduction

Lithium-ion batteries (LIBs) have high energy density, long cycling life and cause little pollution [1,2]. Hence, they have become the primary source of energy for a number of applications ranging from portable electronics to battery electric vehicles (BEVs). However, the operating temperatures of LIBs have a significant impact on their performance. At low temperatures, LIBs experience reduced charging efficiency, significant power loss and accelerated aging [3–5]. For BEVs, these effects negatively impact the driving range. Hence, there is a strong need to develop effective battery climatization techniques under low temperature operations for improved battery and vehicle performance.

Several studies have attempted to investigate the battery performance and aging at low temperatures. Nagasubramanian [6] studied the performance of the commercial 18650 Li-ion cell and he reported an energy density of 5% and power density of 1.25% at −40 °C as compared to 25 °C. Zhang et al. [4] linked the poor performance of battery cells at low temperatures to the poor charge transfer at the electrode/electrolyte interface due to slow kinetics. Fan and Tan [7] studied the charging characteristics at low temperatures and found that significant lithium plating, which occurred when charging at low temperatures, led to an irreversible decrease in battery capacity. They also recommended avoiding charging at high current at these temperatures. Bandhauer et al. [8] reviewed the temperature effects on capacity loss and concluded that the charge transfer degraded rapidly with decrease in temperature and that the slow charge transfer at the electrode/electrolyte interface caused the poor low-temperature performance of the cells. Petzl et al. [9] focused on non-destructive characterization of the fading behavior of the battery cells during long-term cycling. They elucidated the lithium plating effects on the graphite anode as the most severe factor leading to capacity fade in LIBs at low temperature, where the loss of cyclable active lithium material led to capacity decay. To summarize, poor performance of LIBs in cold climates can be attributed to four main factors [3–5,8,10–13]: (1) low conductivity of the electrolyte and solid electrolyte interface on the electrode surface; (2) declined solid-state Li diffusivity; (3) high polarization of the graphite anode; and (4) sluggish kinetics caused by high charge-transfer resistance on the electrode interfaces.

In vehicle applications, these factors limit battery discharge during propulsion and their charging ability during regenerative braking. Numerous studies have investigated battery modeling for vehicle applications and have attempted to capture these effects both numerically and experimentally [14–23]. Shidore and Bohn [14] quantified the

☆ This document is the result of the research project funded by the Swedish Energy Authority/FFI project number, D. nr P48024-1.
* Corresponding author.
E-mail address: anandh.rameshbabu@chalmers.se (A. Ramesh Babu).

https://doi.org/10.1016/j.applthermaleng.2022.118548
Received 12 January 2022; Received in revised form 8 April 2022; Accepted 17 April 2022
Available online 4 May 2022

Nomenclature

Abbreviations

LIB	Lithium-ion battery
BEV	Battery electric vehicle
PCM	Phase-change material
ECM	Electrical circuit model
EPA	Environmental energy agency
HWFET	Highway fuel economy test
NMC	Nickel–Manganese–Cobalt
1D	One-dimensional
RC	Resistance–capacitance
RMS	Root mean square
CFD	Computational fluid dynamics
HPPC	Hybrid pulse power characterization

Symbols

τ	Motor torque
ω	Motor angular velocity
M_v	Mass of the vehicle
P	Traction power
a_v	Vehicle acceleration
ρ_a	Density of air
v_v	Vehicle velocity
C_d	Coefficient of drag
A_{f_v}	Vehicle frontal area
μ_r	Rolling resistance
g	Acceleration due to gravity
α	Road gradient
$R_{i,0}$	Battery resistances
C_i	Battery capacitances
V_T	Terminal voltage
U_{oc}	Open-circuit voltage
U_i	Voltage drop across i_{th} RC branch
SoC	State of charge
I	Current
Δt	Timestep size
Q	Heat rejected by each module
N_{mod}	Number of cells in each module
T	Temperature
$\frac{dU_{oc}}{dT}$	Battery entropic coefficient
t	Encapsulation thickness
k	Thermal conductivity
ρ	Density
c_p	Specific heat
R_{th}	Thermal resistance
C_{th}	Thermal capacitance
T_∞	Ambient temperature
$\Delta T_{w-\infty}$	Difference between wall and ambient temperatures

impact of low ambient temperatures 0 °C and −7 °C on battery performance in hybrid electric vehicles. They found a 34% reduction in battery power and an 8%–12% increase in internal resistance at these temperatures as compared to an ambient temperature of 20 °C. Moreover, battery packs not only provide energy to power the propulsion system, but also acclimatize themselves, the entire powertrain and the passenger compartment. At low temperatures, a large portion of the energy is spent on heating the battery packs and the cabin, thus shortening the driving range by more than 30%–40% [16,18]. Taggart [22] analyzed over 10,000 T Model S and observed energy consumption increased by over 45% at −10 °C. Short trips particularly exhibited higher consumption due to the transient battery and cabin heating energy demand. Steinstraeter [23] et al. studied the impact of cabin heating demand and limited battery capacity to recuperate energy at low temperatures in the Tesla Model 3 and in the BMW i3. The results showed a 32% decrease in range due to heating demand and a 22% decrease due to limited recuperation, giving a combined maximum decrease of about 50% under cold conditions. This emphasizes the need for efficient vehicle thermal management systems to improve low-temperature performance and prolong the range in BEVs.

To overcome the challenges at low-temperature operating conditions, different strategies have been studied both experimentally and numerically. Battery heating is a feasible approach that has been extensively studied to improve the low-temperature performance of LIBs. Battery heating strategies were first investigated by Pesaran et al. [24,25]. They classified battery heating based on energy source and energy/heat transfer pattern and compared different heating strategies to improved battery performance. Later, Wang et al. [5] classified methods with respect to the location of heat generation into ‘internal’ and ‘external’ methods, where internal methods use the cell’s internal resistance to heat themselves up while the external methods use heat generated outside the cells to warm up either convectively or conductively. Ji and Wang [26] employed an electrochemical-thermally coupled model to simulate the different heating processes, namely self-heating, convective heating, pulse heating and externally powered heating, from subzero temperature. Their characteristics were discussed in terms of capacity loss, time and cost. They observed that the pulse heating strategy produced the least capacity loss, which implied an increase in vehicle range. With the convective and pulse heating methods, the warm-up time was reduced considerably. Other studies [27,28] have performed similar investigations to corroborate the findings on the aforementioned heating strategies. The usage of heat pumps [16,18,29,30] and battery pre-conditioning coolant circuit [18] have been explored to reduce the load on batteries for self-heating during vehicle operation. Nevertheless, heating with external power supply proved to be the best solution since it produced the least capacity loss and long cycling life [26,31–33]. While there has been a considerable effort towards improving the warm-up performance of batteries using different strategies, a few studies have examined passive thermal management such as battery insulation to reduce heat loss at low ambient temperatures. Hu et al. [34] pointed out that effective insulation can reduce heat loss to the environment, thus reducing the energy expenses during the warm-up phase. Recently, Ouyang et al. [35] carried out a series of experiments to probe the influence of thermal insulation around battery cells for the temperature range 0–20 °C and concluded that thermally insulated cells showed improved discharge performance and a slower decay rate. Ling et al. [36] investigated the effect of phase change materials (PCM) with high thermal capacitance to store heat. It was noted that the usage of PCM decreased the rate at which the cells cool down, but negatively affected the heat-up performance of already cold battery cells. Wu et al. [37] examined the effect of thermal insulation using nano-porous aerogel with different thickness in battery cells. The low thermal diffusivity of the aerogel aided in retaining heat in the cells at low temperatures resulting in better energy utilization.

With the available literature indicating that insulating battery packs can be beneficial while operating under low ambient temperatures, the effect of battery pack insulation at the vehicle level and the potential energy savings under drive cycle conditions is yet to be investigated. This paper focuses on a numerical study of battery pack thermal encapsulation and its effect on the energy usage of electric vehicles under parking–driving scenarios at low ambient temperatures. The vehicle energy consumption of an encapsulated battery pack was compared to a non-encapsulated pack, and a parametric analysis was performed by varying the material properties and thickness of the thermal encapsulation.

Table 1
Truck specifications.

Parameter	Value
Vehicle mass (M_v)	15000 kg
Tyre rolling resistance (μ_r)	0.008
Drag coefficient (C_d)	0.5
Frontal area (A)	10 m^2
Gear-train efficiency (η_{gt})	0.95

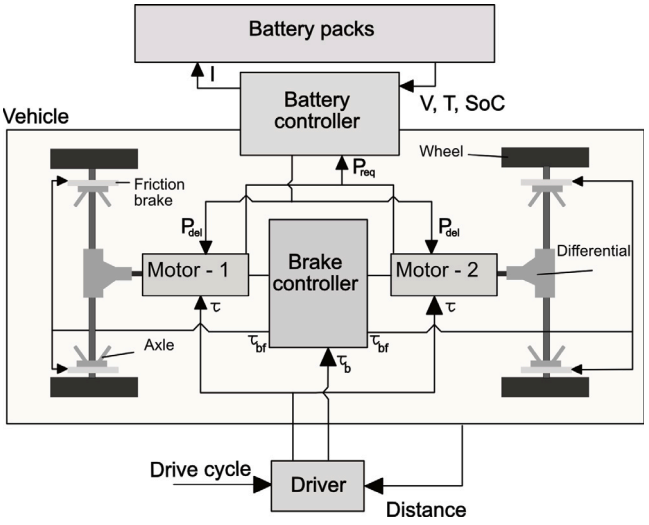

Fig. 1. Schematic of the electric truck model.

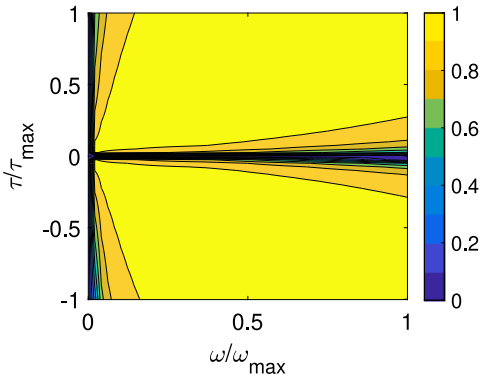

Fig. 2. Electric machine efficiency map.

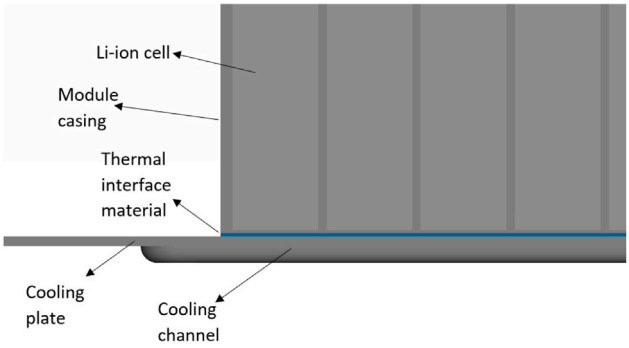

Fig. 3. Cross-sectional view of the battery module.

2. Modeling methodology

To perform transient drive cycle simulations, a system-level vehicle model was developed in GT-SUITE, a commercial simulation platform for vehicle systems [38]. This section describes in detail the vehicle model comprising the electric energy storage (battery packs), the electric powertrain, the cooling system and the vehicle controllers.

2.1. Vehicle model

The vehicle considered in this work was a simplified fully electric truck (see schematic in Fig. 1) and its main specifications are presented in Table 1. It had two axles, each driven by an electric motor through a differential. The electric motors served also as generators to regenerate energy while braking. The efficiency map of the electric machine as a function of operating torque (τ) and angular velocity (ω) is shown in Fig. 2. The traction power was calculated as:

$$P = \left(M_v a_v + \frac{1}{2}\rho_a v_v^2 C_d A_{f_v} + (\mu_r \cos(\alpha) + \sin(\alpha)) M_v g \right) v_v \quad (1)$$

The vehicle was driven by a driver model which requested torque (accelerating or braking) from the electric machines to match the actual vehicle speed with the prescribed speed (drive cycle). Based on the operating angular velocity, torque and efficiency, the electric machines requested/delivered electrical power from/to the battery pack controller. The battery controller (further explained in the later subsection) converted this power into current that discharged/charged the battery packs. The output power from the battery packs was sent back to the electric machines to drive the vehicle. In case the power delivered was lower than the power requested, the vehicle acceleration was reduced and the target speed would not be achieved. During braking, the brake controller unit received information about the maximum power that could be harnessed by the batteries to be stored (charging threshold) and the maximum braking torque the motors could produce. If the regenerated power was lower than the maximum charging threshold, the batteries were charged whereas if the regenerated power exceeded the maximum threshold, the batteries charged at their limits and the rest of the braking torque was supplied by friction brakes. The driver model received information about the position of the vehicle to satisfy the total distance traveled as a result of the prescribed speed profile.

2.2. Battery pack modeling

The battery pack modeling employed strategy for thermal simulations in this work was presented by the authors in their previous publication [39]. The paper discusses the modeling approach of different components, calibration and validation with four experimental test data for the battery pack. Nevertheless, a brief description of the battery pack geometry and the modeling approach is provided here for completeness. The vehicle energy storage system consisted of three battery packs with configuration 180s2p (where s stands for series and p stands for parallel). Each pack contained two trays, placed one on top of the other. Each tray included battery modules, an aluminium cooling plate and a thermal interface material separating the module casings and the cooling plate as shown in Fig. 3. Every module had several prismatic NMC cells with the specifications tabulated in Table 2. The cooling channels were stamped on the cooling plate and indirectly cooled/heated the battery cells. Heat conduction was modeled between the battery cells and the cooling plates. The coolant flow through the cooling channels was described using the 1D Navier–Stokes equations and the heat transfer between the cooling plate and the cooling channels was modeled using the empirical Colburn expression [40].

Electrical circuit model

A second-order Thevenin electrical circuit model (ECM) [41] was used to describe the electrical behavior of battery cells together with Bernardi's thermal model [42] to account for heat generation. The ECM uses resistors (R_i) and capacitors (C_i) to estimate the output voltage.

Table 2
Battery cell specifications.

Parameters	Values
Cell type	Li-ion NMC
Rated capacity	37 Ah
Nominal voltage	3.7 V
Minimum voltage	3 V
Maximum voltage	4.2 V
Specific heat	1145 J/kgK
Density	1827 kg/m^3
Thermal conductivity	19.3 W/mK

Table 3
RMS error of the normalized battery pack output voltage.

Case-1	Case-2	Case-3
0.567%	0.699%	0.973%

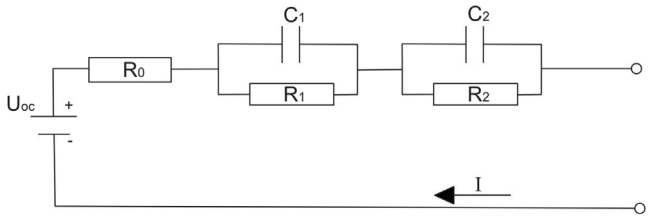

Fig. 4. Schematic of the second-order Thevenin electrical circuit model.

The schematic of the second-order Thevenin ECM is illustrated in Fig. 4. The output voltage V_T is computed as [43]:

$$U_i(j+1) = U_i(j)e^{-\frac{\Delta t}{R_i C_i}} + R_i(1 - e^{-\frac{\Delta t}{R_i C_i}})I(j) \quad (2)$$

where i∈[1,2] and,

$$V_T(j) = U_{oc} - U_1(j) - U_2(j) - R_0 I(j) \quad (3)$$

Look-up tables as functions of current, battery temperature and SoC were created for the model parameters $R_{i,0}$ and C_i by using a standard hybrid pulse power characterization (HPPC) test of the battery cell. The developed model was applicable for cell temperatures between −30 °C to 50 °C across SoC in the range of 0.1 to 0.9 and at different current rates. Nevertheless, the battery pack model was discretized at the module level. All battery cells within the same module were assumed to have identical states. Each module was considered as one thermal mass. The heat generated (Q) by each module was estimated using the expression:

$$Q = N_{mod} I \left((U_{oc} - V_T) + T \frac{dU_{oc}}{dT} \right) \quad (4)$$

The battery pack model was validated for three cyclic charge–discharge current profiles. The simulation results for the battery pack terminal voltage were compared with the experimental measurements. The current profiles had a maximum current of 2 C (where C represents C-rate which is the charge/discharge current relative to the battery capacity) during charge and discharge, and they each varied in frequency. The root mean square (RMS) error was computed for the three cases (see Table 3). The ECM marginally under-predicted the average battery pack voltage with the maximum RMS error of 1%.

Battery pack cool-down

The battery pack casing was a 3 mm thick stainless steel plate enclosing the battery modules. The heat transfer between the battery casing and the surrounding air occurs due to convection and the framework being 1D, the heat transfer coefficient (h_∞) at the wall must be specified. The heat transfer coefficient between the battery casing and the environment was estimated using the results from CFD simulations of a simplified battery pack geometry. The CFD simulations were performed for various battery pack wall temperatures and surrounding air temperatures, and a lookup table for the difference in wall temperature and air temperature ($\Delta T_{w-\infty}$) versus average wall heat transfer coefficient was obtained. Thus in the 1D simulations, based on the instantaneous $\Delta T_{w-\infty}$, the h_∞ value was imposed.

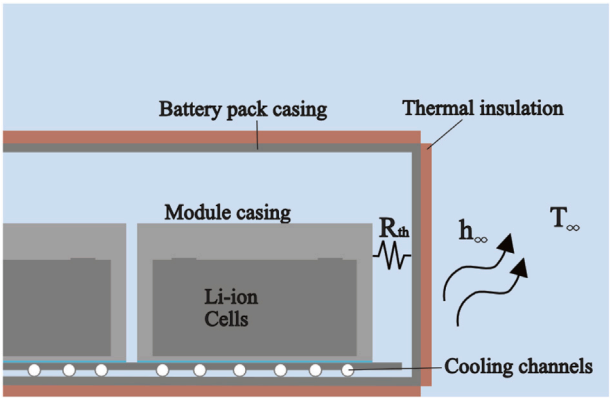

Fig. 5. Thermal encapsulation of the battery pack.

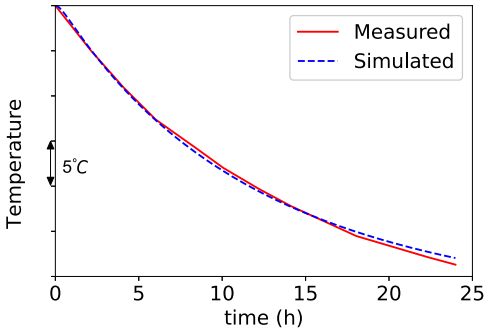

Fig. 6. Average battery pack temperature during cool-down at the ambient temperature −15 °C.

The heat transfer between the modules and the battery pack casing was modeled using a thermal resistance (R_{th}) (see Fig. 5). By using thermal resistance, the geometric effects were simplified within the pack and the thermal resistance of the intermediate air between the modules and the battery casing could be accounted for. The thermal resistance was calibrated using the temperature measurement data from a cool-down test of the battery pack, that was performed by the supplier. In this test, the battery pack initially at an optimal operating temperature, was allowed to cool down by natural convection at an ambient temperature of −15 °C and the average battery pack temperature was monitored for 24 h. The thermal resistance was optimized using the Nelder–Mead optimization approach [44] so that the difference between the simulated and the measured temperature values was minimized. Fig. 6 illustrates the agreement between the measured and simulated average battery pack temperatures during cool-down. The RMS error between the simulated and measured temperatures is 0.35 °C.

Thermal encapsulation of the battery pack

All three battery pack casings were encapsulated using thermal insulation materials as seen in Fig. 5. A plate of thermally insulating material of certain thickness and material properties (discussed later in Section 3) was placed on each side of the battery pack. The thermal conduction between the battery pack casing and the thermal insulation was considered. The net increase in the truck's total mass due to the presence of the insulating material was taken into account when calculating the power request.

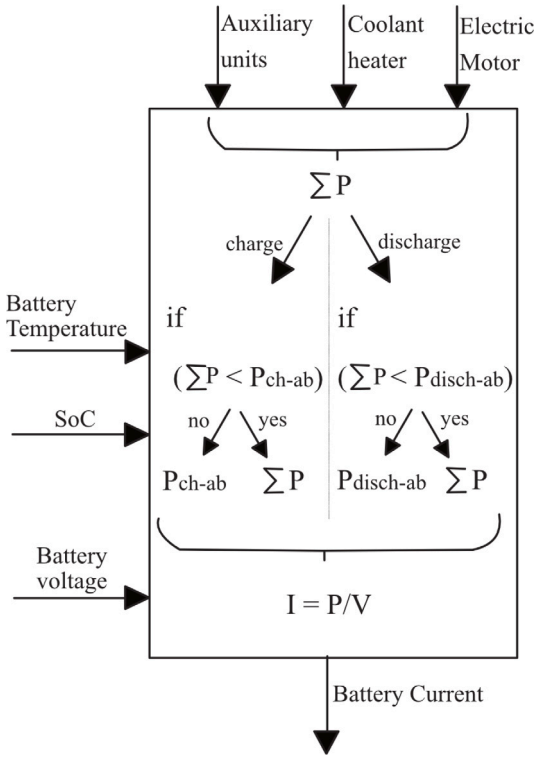

Fig. 7. Battery pack control unit.

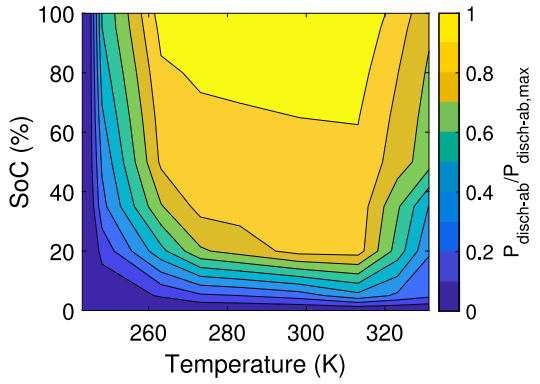

Fig. 8. Normalized battery discharge ability ($P_{disch-ab}/P_{disch-ab,max}$) as a function of SoC and temperature.

Battery pack control unit

The simplified control logic for the battery pack simulations is shown in Fig. 7. The electrical power was requested/delivered from/by the electric motor-generator unit. This power was then converted to discharge/charge current based on the battery's output voltage. In addition, the battery pack's maximum discharge/charge ability was considered in terms of power as a function of temperature and SoC as seen in Figs. 8 and 9, respectively. When the coolant heaters were engaged to heat up the battery packs, this power demand in addition to the request from the traction components and the auxiliary units was also considered.

2.3. Energy storage cooling system

The schematic of the cooling system for the electric energy storage is presented in Fig. 10. A pump was used to climatize the three battery packs in the truck during operation. Battery-1 and Battery-2 were

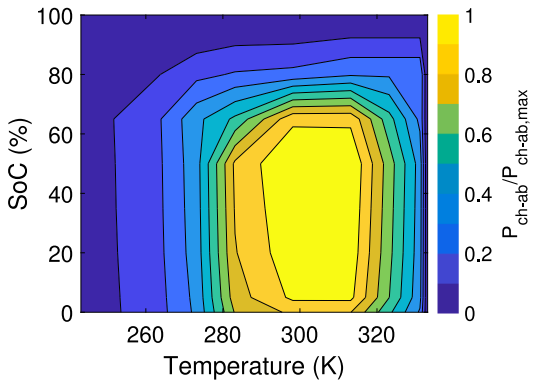

Fig. 9. Normalized battery charge ability ($P_{ch-ab}/P_{ch-ab,max}$) as a function of SoC and temperature.

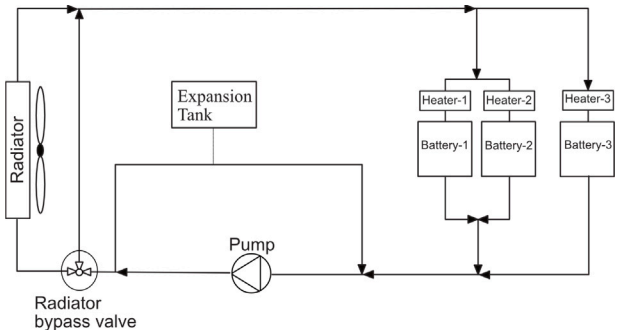

Fig. 10. Schematic of the electric energy storage cooling circuit.

placed on the right side of the vehicle while Battery-3 was placed on the left-side and hence the coolant hoses were modeled as shown in the figure. A 2.5 kW coolant heater was placed in front of each battery pack to supply heat in case their temperatures fell below a threshold value. The ideal battery operating temperature range is 15 to 35 °C [45,46] and therefore the threshold temperature was set to 15 °C. Additionally, a radiator bypass valve was used to regulate the coolant flow through the radiator. In the cases that either the coolant heaters were engaged or the average temperature of the packs fell below 25 °C, the flow was bypassed from the radiator whereas if the temperature of the battery packs was above 25 °C, the bypass valve was shut off and the coolant flowed through the radiator. A fan was placed in the under-hood compartment downstream of the radiator. The fan was used when the ram air was less than 15 km/h and if there was coolant flow in the radiator. Finally, an expansion tank was included in the circuit to prevent over-pressure due to coolant expansion under heating or to supplement the primary system with additional coolant when coolant contracts under cooling, which would otherwise create a negative pressure. The power required to run the fan and pump were included as auxiliary units in the battery controller (see Fig. 7).

3. Simulation methodology

The truck simulations were performed for the EPA HWFET driving schedule (see Fig. 11). The battery packs without thermal encapsulation were considered and referred to as the baseline configuration. The simulations were performed to investigate:

1. Temperature influence of the battery pack performance
2. Influence of battery pack encapsulation on parking–driving scenarios at different ambient temperatures
3. Parametric analysis of encapsulation characteristics

In all the simulations, the initial SoC for the battery packs was 80%.

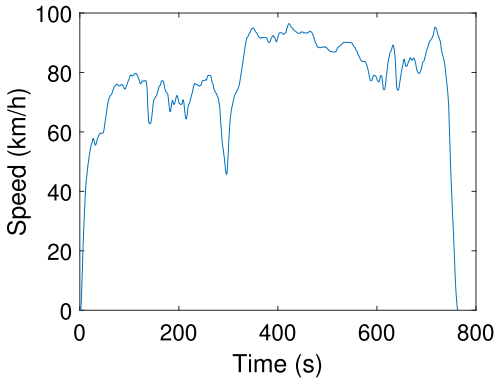

Fig. 11. EPA HWFET drive cycle; Duration—765 s; Distance—16.45 km; Average speed—77.7 km/h [47].

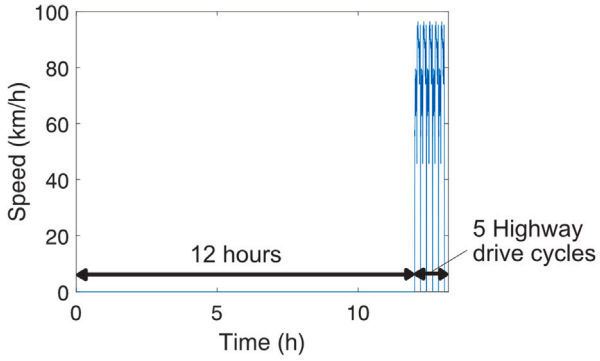

Fig. 12. Drive cycle with cool-down.

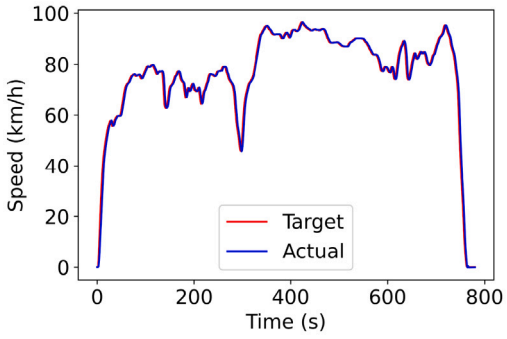

Fig. 13. A comparison between the target and simulated speed of the truck for the HWFET drive cycle.

Table 4
Battery pack encapsulation characteristics.

Property	Value
Density (ρ)	61 kg/m^3
Thermal conductivity (k)	0.027 W/mK
Specific heat (c_p)	2500 J/kgK
Encapsulation thickness (t)	0.0127 m

Table 5
Sensitivity analysis of the encapsulation thickness and material properties of the insulating material.

Property	Values
Encapsulation thickness (m)	0.00635, 0.0127, 0.0254, 0.0508
Thermal conductivity (W/mK)	0.001, 0.01, 0.1, 1
Density (kg/m^3)	30, 60, 120, 240, 480
Specific heat (J/kgK)	500, 1000, 2000, 4000

3.1. Temperature influence on the battery pack performance

Five different battery initial operating temperatures, 40 °C, 25 °C, 10 °C, 0 °C and −10 °C were considered to assess the performance of the battery pack in the baseline configuration. The coolant heaters were not used in this study. The voltage output from the battery pack, the current requested/delivered and the average energy consumption during the drive cycle were analyzed.

3.2. Influence of battery pack encapsulation on parking–driving scenarios at different ambient temperatures

A parking–driving scenario consisting of a 12-hour parking period followed by five consecutive HWFET cycles was considered as seen in Fig. 12. The simulations were performed at five ambient temperatures, 25 °C, 10 °C, 0 °C, −10 °C and −25 °C, with the initial battery pack temperature at 25 °C. The coolant heaters were engaged to heat the battery packs if necessary, when the driving phase started. As previously mentioned, the coolant heaters were turned on when the battery pack temperatures were below 15 °C. Both the baseline configuration and the encapsulated battery packs were examined. The information about the encapsulation thickness and the properties of the commercially available insulating material [48,49] are presented in Table 4.

3.3. Parametric analysis of encapsulation characteristics

Finally, the encapsulation thickness and the material properties of the encapsulation material (see Table 5) were varied to analyze their effects on the pack's performance in cold climates. Three ambient temperatures, 0 °C, −10 °C and −25 °C were considered and the same parking/driving scenario with battery packs at 25 °C initial temperatures was simulated as presented in Fig. 12. Only one property was varied at a time. The variation in the truck's mass due to changes in the encapsulation mass (material density and encapsulation thickness) was considered when calculating traction power. The battery pack temperature at the end of the parking phase, the energy consumed by the coolant heaters, the average energy consumption during the drive cycle and the percentage of energy savings relative to the baseline configuration were used to assess the performance of each design configuration.

4. Results and discussion

Fig. 13 shows an excellent agreement between the target and the simulated speed when the truck is run through the HWFET drive cycle. Based on the driver's torque request from the electric motors, the electric motors' power request from the batteries, and the batteries' operating characteristics, the target vehicle speed is achieved.

4.1. Temperature influence of the battery pack performance

Figs. 14 and 15 present the variations in the output voltage and discharge/charge currents respectively, during the HWFET drive cycle. Note that the negative values represent discharge currents and positive values, charge currents.

A decrease in the output voltage is observed with a decrease in the battery pack temperature. The output voltage is a function of the internal battery resistance and a decrease in the operating temperature leads to an increase in the internal resistance which results in lower output potential. Consequently, higher discharge currents are required at lower operating temperatures to satisfy the power demand (see Fig. 15). At the same time, the charging ability of the batteries during regenerative braking is reduced at these temperatures which translates

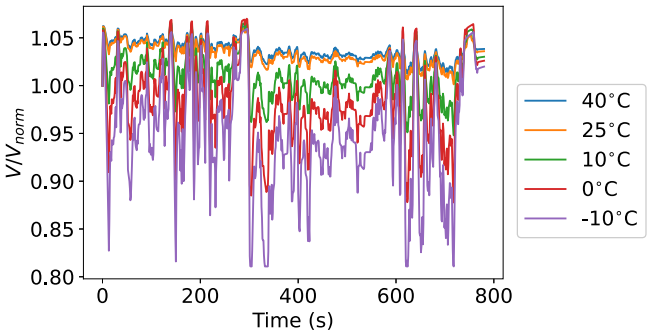

Fig. 14. Output voltage from the battery pack for HWFET drive cycle at different operating temperatures.

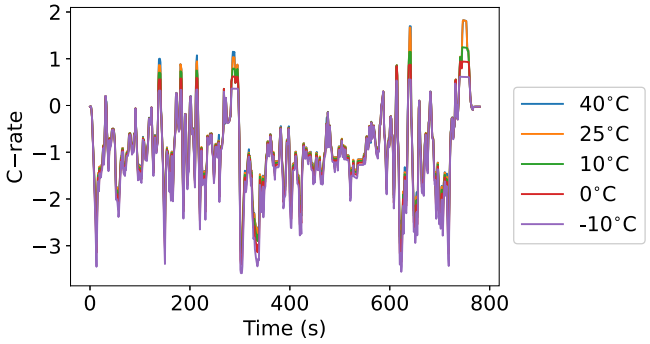

Fig. 15. Current requested from/delivered to the battery pack at different operating temperatures.

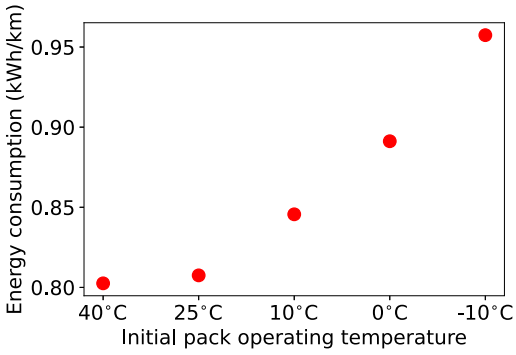

Fig. 16. Average truck energy consumption during the HWFET driving cycle for different pack operating temperatures.

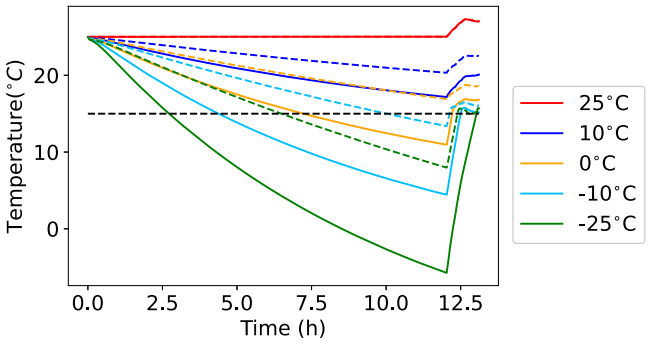

Fig. 17. Average battery pack temperature; Baseline configuration (-), Encapsulated configuration (––).

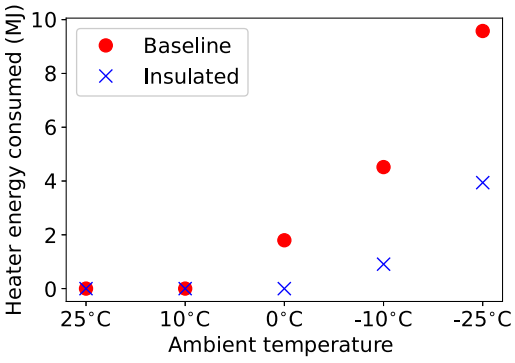

Fig. 18. Energy consumed by the coolant heater to heat up the battery pack.

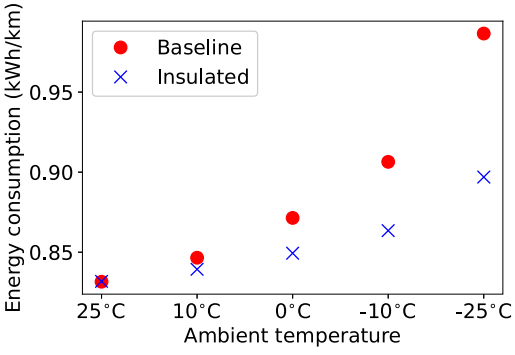

Fig. 19. Average vehicle energy consumption during the parking–driving scenario.

to lower current input during charging (see Fig. 9). Thus, the battery discharges more and recovers lesser energy while operating at low temperatures. Fig. 16 illustrates the relationship between the average energy consumption of vehicle and the battery pack operating temperature during the HWFET drive cycle. An increase in the average energy consumption with a decrease in operating temperature is seen for the operating temperatures below 25 °C because of the above-mentioned effects. The battery pack consumes an average of 0.15 kWh/km (18.7%) more at −10 °C as compared to the pack operating at 25 °C.

4.2. Influence of battery pack encapsulation on parking–driving scenarios at different ambient temperatures

The average battery pack temperatures under parking–driving scenario at different ambient temperatures are presented in Fig. 17. The battery pack temperature was initialized to 25 °C. The horizontal black dotted line represents the 15 °C temperature threshold for battery pack heating during its operation. It is observed that the encapsulated battery pack retains higher temperatures (dotted lines) compared to the baseline configuration (solid lines) at all ambient temperatures except 25 °C where the initial pack and ambient temperatures are equal. This effect is seen because of the additional thermal insulation between the battery pack casing and the ambient, which reduces the heat transfer between the battery modules and the cold environment.

The energy provided by the coolant heater to heat the battery pack at different ambient temperatures is shown in Fig. 18. The energy consumed by the coolant heaters increases for both the encapsulated and the baseline configurations at the ambient temperatures −10 °C and −25 °C. But with battery pack encapsulation, the energy requirement is reduced since the battery packs are at higher temperatures at the end of the parking phase. At 0 °C, the encapsulation acclimatizes the battery pack above the 15 °C threshold, thereby eliminating the need for heating whereas the baseline battery pack requires about 2 MJ of energy to heat the battery pack to 15 °C.

Table 6
Percentage of energy savings with the encapsulated pack relative to the baseline configuration at different ambient temperatures.

Ambient temperature (°C)	Energy savings (%)
25	−0.03
10	0.85
0	2.53
−10	4.74
−25	9.08

Table 7
Increase in the mass of the truck due to increase in the encapsulation thickness.

Thickness (m)	Mass increase (kg)
0.00635	4.6
0.0127	9.2
0.0254	18.4
0.0508	36.8

Fig. 19 and Table 6 illustrate the average truck energy consumption during the driving phase and the percentage of energy saved with the encapsulated configuration relative to the baseline configuration, respectively. The average energy consumption for the vehicle increases with decrease in the ambient temperature for both the insulated and baseline battery packs. This is observed because of the increased battery internal resistance and reduced charging capacity at low battery operating temperatures, as discussed in Section 4.1. Nonetheless, the combined effects of higher pack operating temperature and reduced energy expenses for the coolant heaters, the vehicle with the insulated battery packs consumes lesser energy overall, at all low ambient temperature scenarios (10 °C, 0 °C, −10 °C and −25 °C). At 25 °C ambient however, the energy consumed is marginally (0.03%) higher for the vehicle with the encapsulated configuration due to the increased truck mass. Nevertheless, the energy saved increases for the encapsulated configuration with a decrease in ambient temperature from 0.8% at 10 °C to about 9% at −25 °C. The results demonstrate the feasibility of using thermally insulating materials around the battery pack casing as opposed to insulating individual cells as performed in other studies [35–37] which can pose design and packaging constraints especially in large packs that are tightly packed to increase the energy density.

4.3. Parametric analysis of the encapsulation characteristics

The results from Section 4.2 demonstrate the feasibility of battery pack encapsulation as a means to climatize the battery pack under parking–driving scenarios at low ambient temperatures. In this subsection, the encapsulation characteristics are varied to study their influence on the vehicle energy consumption.

4.3.1. Effects of variation in the encapsulation thickness

The thickness of the encapsulation was varied as specified in Table 5, while the material properties were retained (see Table 4). The increase in the mass of the insulating material with varying thickness is tabulated in Table 7.

The average battery pack temperature at the end of the 12-hour parking period at different ambient temperatures is presented in Fig. 20. It is seen that thicker encapsulation yields higher average battery pack temperatures at the end of the parking period for all ambient temperatures because of the decrease in heat transfer between the battery modules and the ambient. The horizontal black dotted line represents the threshold temperature of 15 °C for engaging coolant heaters during the truck operation. Consequently, the energy required to heat the battery pack decreases with an increase in the encapsulation thickness as seen in Fig. 21. With the encapsulation thickness of 0.0508 m, the need for battery pack heating is eliminated at all

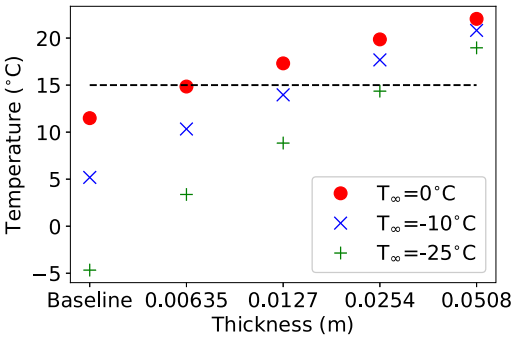

Fig. 20. Average battery pack temperature at the end of the 12-hour parking period with variation in the encapsulation thickness at different ambient temperatures.

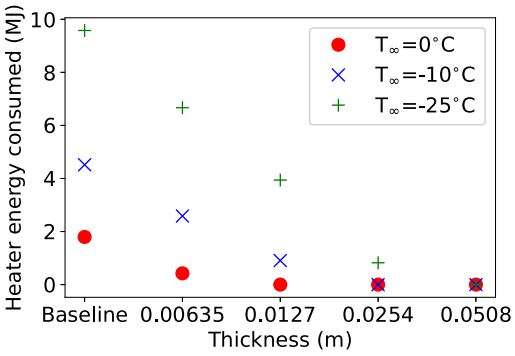

Fig. 21. Coolant heaters energy usage during the driving phase with variation in the encapsulation thickness at different ambient temperatures.

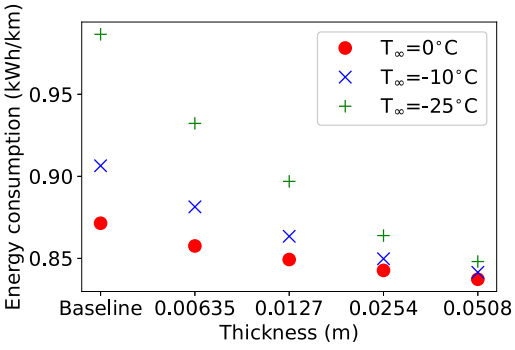

Fig. 22. Average vehicle energy consumption during the parking–driving scenario with variation in the encapsulation thickness at different ambient temperatures.

considered ambient temperatures and with a thickness of 0.0254 m, battery pack heating is required only at the ambient temperature of −25 °C.

The decreased energy usage of the coolant heaters with thicker pack encapsulation and higher overall battery pack temperature during the cycle result in reduced average energy consumption as seen in Fig. 22. Minor variations in the average energy consumption are observed for all cases even though the coolant heaters are not used. This is a result of the slightly reduced performance due to lower battery temperature as explained in Section 4.1 and additional power requirements as a result of the varying truck mass due to encapsulation. The percentage of energy savings with varying encapsulation thickness relative to the baseline energy consumption at different ambient temperatures is shown in Table 8. The magnitude of energy savings increase with decrease in ambient temperature as seen in Section 4.2 and with increase in encapsulation thickness. Thus, the benefit of increased thickness,

Table 8
Percentage of energy savings with variation in the encapsulation thickness at different ambient temperatures.

T_∞	Encapsulation thickness (m)			
	0.00625	0.0127	0.0254	0.0508
0 °C	1.58	2.53	3.29	3.91
−10 °C	2.76	4.74	6.25	7.16
−25 °C	5.50	9.08	12.43	14.03

Table 9
Percentage of energy savings with variation in the thermal conductivity of the encapsulation material at different ambient temperatures.

T_∞	Thermal conductivity (W/mK)			
	0.001	0.01	0.1	1
0 °C	4.43	3.59	0.71	−0.62
−10 °C	8.09	6.67	1.28	−1.33
−25 °C	15.41	13.31	2.66	−1.85

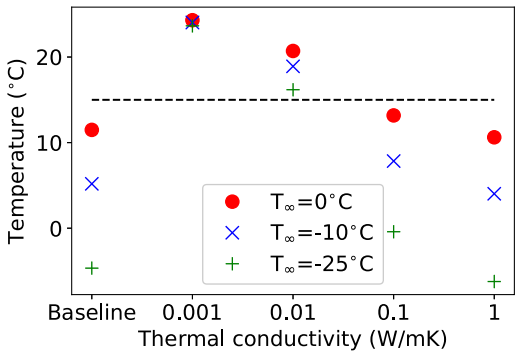

Fig. 23. Average battery pack temperature at the end of the 12-hour parking period with variation in the thermal conductivity of the material at different ambient temperatures.

which reduces heat loss to the environment, outweighs the negative impact of the increased mass of the truck.

4.3.2. Effects of variation in the thermal conductivity of the encapsulation material

The thermal conductivity of the insulating material was varied as specified in Table 5. Fig. 23 displays the average temperature of the battery pack at the end of the 12-hour parking period.

With low thermal conductivity of the material, the ability of the material to conduct heat conduction is reduced, which reduces the rate of heat transfer between the battery modules and the ambient. This results in higher temperature of the battery pack. With an increase in the thermal conductivity, the average temperature of the pack decreases as more heat can be rejected through the encapsulation into the ambient. When the thermal conductivity approaches 1 W/mK, the encapsulated pack temperature decreases and reaches a value lower than the baseline configuration during cool-down which means the encapsulation enhances the heat transfer to the ambient, and thus acts as a fin.

The energy consumed by each coolant heater with changes in the thermal conductivity of the encapsulation material is shown in Fig. 24. It is seen that for thermal conductivity of 0.001 W/mK, the pack temperature stays above the threshold value for all ambient temperatures, and hence the heaters are not engaged. With increase in the thermal conductivity of the material, which results in lower temperatures of the battery pack at the end of the parking phase, the magnitude of heater energy consumed increases. Consequently, the average energy consumption of the vehicle increases with increase in the thermal conductivity of the encapsulation as illustrated in Fig. 25.

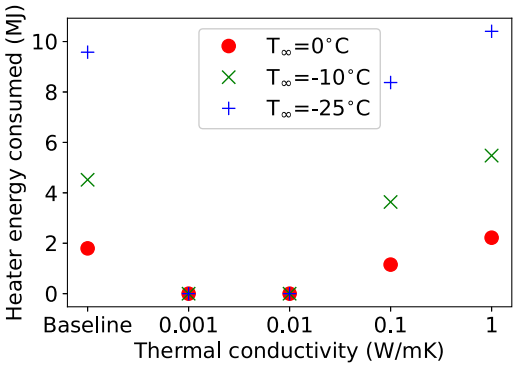

Fig. 24. Coolant heaters energy usage during the driving phase with variation in the thermal conductivity of the material at different ambient temperatures.

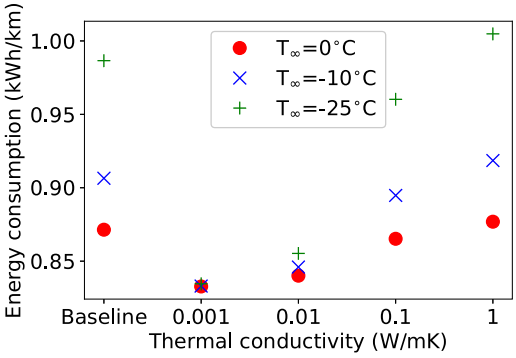

Fig. 25. Average vehicle energy consumption during the parking–driving scenario with variation in the thermal conductivity of the material at different ambient temperatures.

Table 9 presents the percentage of energy savings with variations in the thermal conductivity of the encapsulation material at different ambient temperatures. Large changes in the percentage of energy savings are seen for variation in the thermal conductivity at respective ambient temperatures, which highlight the importance of this material property while insulating the battery pack. The thermal conductivity of 0.001 W/mK reduces energy consumption by 15.41% while a thermal conductivity of 1 W/mK increases energy consumption by 1.85% at −25 °C relative to the baseline configuration.

Effects of the thermal resistance of the encapsulation material

The energy savings from Sections 4.3.1 and 4.3.2 have been plotted against the thermal resistance ($R_{th} = t/k$) in Fig. 26 at different ambient temperatures. It can be seen that the energy savings increases when the thermal resistance of the encapsulation material is increased till approximately 2 Km^2/W beyond which the energy savings become asymptotic. As previously explained, with decreasing the thermal conductivity or increasing the thickness (resulting in high thermal resistance), the heat loss to the surroundings is reduced resulting in higher battery pack temperatures at the end of the parking phase. However, with thermal resistances above 2 Km^2/W, the temperatures approach closer to the initial battery pack temperature (25 °C). This leads to the average energy consumption approaching 0.83 kWh/km (from Fig. 19), which corresponds to the consumption at 25 °C during the entire cycle. Thus, the asymptotic relationship is seen beyond 2 Km^2/W. The observed results are in-line with the conclusions from [37] where a critical thickness of nano-porous aerogel for cell insulation was suggested beyond which the gains were marginal for a specific operating scenario.

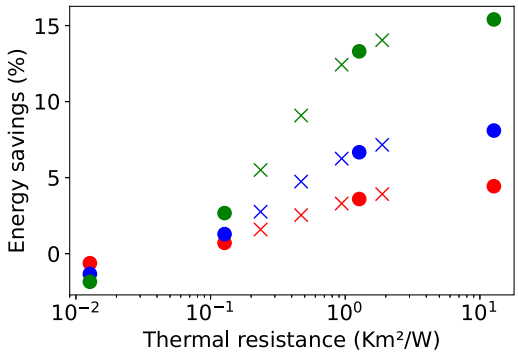

Fig. 26. Effect of thermal resistance on energy savings. ●: variation of thermal conductivity; ×: variation of thickness; red: T_∞ = 0 °C; blue: T_∞ = −10 °C; green: T_∞ = −25 °C.

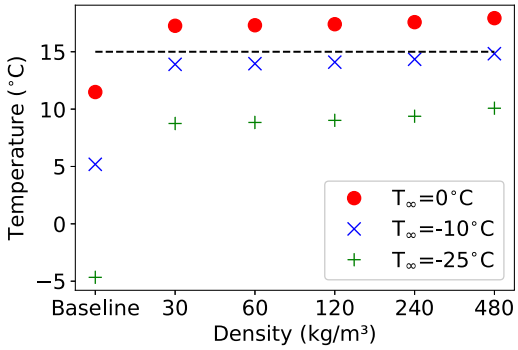

Fig. 27. Average vehicle energy consumption during the parking–driving scenario with variation in the density of the material at different ambient temperatures.

4.3.3. *Effects of variation in the density of the encapsulation material*

The density of the insulation material was varied as shown in Table 5. Table 10 presents the increase in the mass of the truck due to the variation in the encapsulation material density. Fig. 27 displays the temperature at the end of the 12-hour cool-down period at different ambient temperatures. It is noted that the temperatures increase slightly with the increase in density. This corresponds to a small decrease in the total heat rejected by the battery modules to the ambient with increase in the encapsulation density. This effect is observed because of an increase in thermal inertia with the increase in density and therefore, higher thermal energy is stored in the encapsulating material shielding the pack which delays the battery pack from losing heat.

The coolant heater energy consumption for each case is shown in Fig. 28. For cases with ambient temperatures 0 °C, the pack temperatures at the end of the parking phase remain above the 15 °C threshold and hence there was no energy consumed by the coolant heaters. At −10 °C and −25 °C, increasing the density of the encapsulation material marginally reduces the heating energy expense.

The average energy consumption of the truck and the percentage of energy saved with variation in the density of the encapsulation material relative to the baseline configuration are presented in Fig. 29 and Table 11, respectively. The variations in the density of the encapsulating material have a small effect on average vehicle energy consumption and energy savings. At −10 °C and −25 °C, the vehicle energy consumption reduces marginally with the increase in density predominantly due to the reduced energy expenses from the coolant heater which also results in a slight increase in energy savings (see Table 11). However, increasing the density at 0 °C has a slightly unfavorable effect on the percentage of energy saved due to the increased mass of the vehicle as the energy saving decreases from 2.53% with a density of 30 kg/m^3 to 2.51% with a density of 480 kg/m^3.

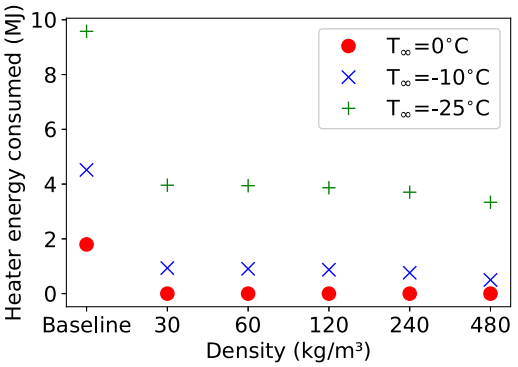

Fig. 28. Coolant heaters energy usage during the driving phase with variation in the density of the material at different ambient temperatures.

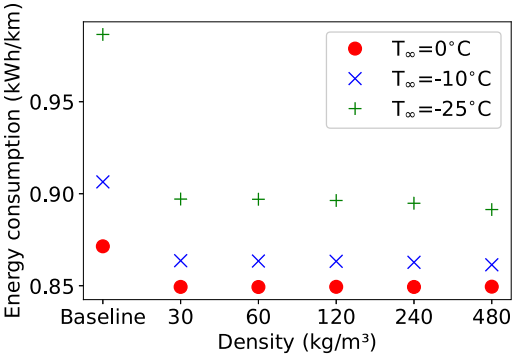

Fig. 29. Average vehicle energy consumption during the parking–driving scenario with variation in the density of the material at different ambient temperatures.

Table 10
Increase in the mass of the vehicle due to increase in the density of the encapsulation material.

Density (kg/m^3)	Mass increase (kg)
30	4.52
60	9.04
120	18.09
240	36.19
480	72.39

Table 11
Percentage of energy savings with variation in the density of the encapsulation material at different ambient temperatures.

T_∞	Density (kg/m^3)				
	30	60	120	240	480
0 °C	2.53	2.53	2.53	2.52	2.51
−10 °C	4.72	4.74	4.76	4.82	4.96
−25 °C	9.06	9.07	9.14	9.29	9.64

4.3.4. *Effects of variation in the specific heat of the encapsulation material*

Finally, the specific heat of the insulating material was varied. The average pack temperatures at the end of the parking phase for each scenario is plotted in Fig. 30. It is seen that the variation in the specific heat of the insulating material has almost no effect on the average pack temperature at the end of the parking phase. Consequently, the heater energy required to heat the battery packs remained approximately equal as seen in Fig. 31.

Fig. 32 and Table 12 exhibit the average truck energy consumption and the percentage of energy savings with variation in the specific heat of the encapsulation material relative to the baseline configuration, respectively. The average energy consumption has a very small decrease with the increase in the specific heat of the encapsulating material at

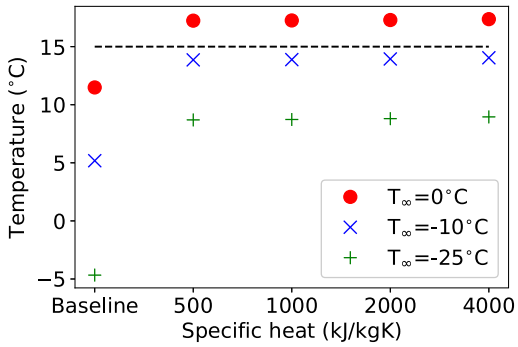

Fig. 30. Average vehicle energy consumption during the parking–driving scenario with variation in the specific heat of the material at different ambient temperatures.

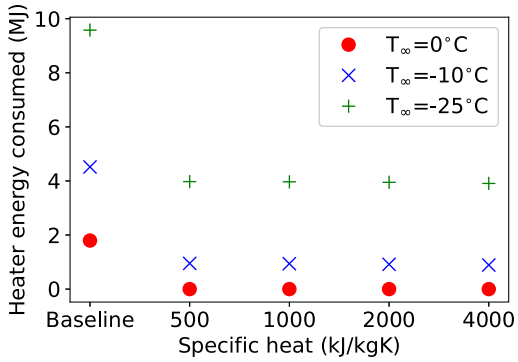

Fig. 31. Coolant heaters energy usage during the driving phase with variation in the density of the material at different ambient temperatures.

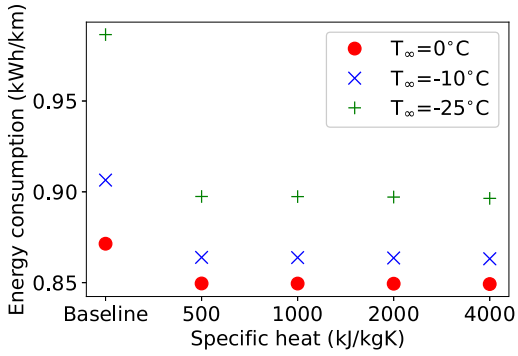

Fig. 32. Average vehicle energy consumption during the parking–driving scenario with variation in the density of the material at different ambient temperatures.

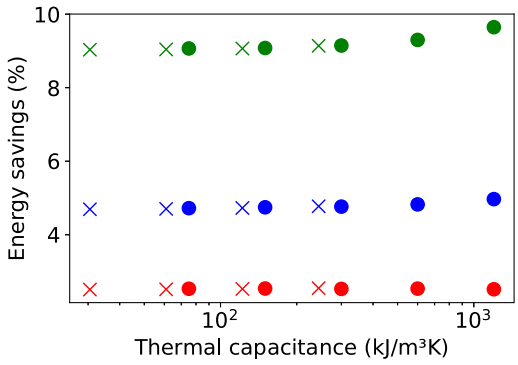

Fig. 33. Effect of thermal capacitance on energy savings. ●: variation of density; ×: variation of specific heat; red: T_∞ = 0 °C; blue: T_∞ = −10 °C; green: T_∞ = −25 °C.

Table 12
Percentage of energy savings with variation in the specific heat of the encapsulation material at different ambient temperatures.

T_∞	Specific heat (kJ/kgK)			
	500	1000	2000	4000
0 °C	2.51	2.52	2.53	2.54
−10 °C	4.69	4.70	4.72	4.77
−25 °C	9.03	9.04	9.06	9.14

all three ambient temperatures considered. The small increase in the energy savings can be attributed to the higher thermal energy stored in the encapsulating material due to the increase in its specific heat thereby delaying the cool down of the battery modules.

Effects of thermal capacitance of the encapsulation

The energy savings from Sections 4.3.3 and 4.3.4 have been plotted against the thermal capacitance ($C_{th} = \rho c_p$) in Fig. 33 at different ambient temperatures. From the plot, it can be seen that the energy savings increased with decrease in the ambient temperature and in the same magnitude as obtained from the study with the commercially available insulating material (see Table 6). However, the increase in the thermal capacitance of the encapsulation has only a marginal effect on the energy savings. As discussed earlier, the higher thermal energy from the encapsulation shields the battery pack and delays it from losing heat. From this plot, it is evident that the battery encapsulation would need significantly large thermal inertia before it can contribute to change in energy savings. Thus, it can inferred that the thermal resistance of the material is responsible for the observed energy savings. Moreover, in the event that the thermal inertia of the encapsulation is depleted, it would then need a large amount of heat energy to heat-up again, which could result in reduced battery performance. This effect was seen when PCM materials [36] that have high thermal capacitance, were used to insulate the batteries, and they negatively impacted the warm-up performance.

5. Conclusions

System simulations were performed for an electric truck to assess its energy usage in cold climates. A thermal encapsulation of the battery packs was emulated and the encapsulation characteristics were varied. The main conclusions from the study are as follows:

1. The energy consumption of the vehicle at −10 °C was 0.15 kWh/km (18.7%) higher as compared to the consumption at 25 °C due to increased internal resistance leading to higher discharge current to satisfy the power demand and decreased charging ability to regenerate energy during braking at low temperatures.
2. The encapsulated battery pack with a commercially available insulating material of thickness 0.0127 m retained a higher temperature compared to the baseline battery pack configuration at all low ambient temperatures during the parking phase. Consequently, the combined effects of improved battery performance and reduced heater usage contributed to lower energy consumption of the truck resulting in about 0.8% at 10 °C to 9% energy savings at −25 °C. Thus if a vehicle was to operate in locations where the average temperature is below the ideal battery operating temperatures (like in northern Europe and America), it would be recommended to encapsulate the battery packs for improved performance.
3. Finally, the thermal resistance of the encapsulation (the thickness and the thermal conductivity of the material) played a significant role in reducing the heat loss from the battery pack to the environment at low ambient temperatures. A thermal resistance of about 2 Km^2/W was found to be sufficient for the battery pack which produced about 4%, 7% and 14% energy savings at 0 °C, −10 °C and −25 °C, respectively.

Declaration of competing interest

The authors declare that they have no known competing financial interests or personal relationships that could have appeared to influence the work reported in this paper.

Acknowledgments

The authors would like to thank Dr. Jelena Andric and Dr. Majid Astaneh, Chalmers University of Technology, and Dr. Masih Khoshab, Volvo Group Truck Technology for their valuable contributions in this work.

References

[1] Y. Azizi, S.M. Sadrameli, Thermal management of a LiFePO4 battery pack at high temperature environment using a composite of phase change materials and aluminum wire mesh plates, Energy Convers. Manage. 128 (2016) 294–302, http://dx.doi.org/10.1016/j.enconman.2016.09.081, URL https://www.sciencedirect.com/science/article/pii/S0196890416308901.

[2] W. Wu, X. Yang, G. Zhang, K. Chen, S. Wang, Experimental investigation on the thermal performance of heat pipe-assisted phase change material based battery thermal management system, Energy Convers. Manage. 138 (2017) 486–492, http://dx.doi.org/10.1016/j.enconman.2017.02.022, URL https://www.sciencedirect.com/science/article/pii/S0196890417301267.

[3] H.P. Lin, D. Chua, M. Salomon, H.C. Shiao, M. Hendrickson, E. Plichta, S. Slane, Low-temperature behavior of Li-ion cells, Electrochem. Solid State Lett. 4 (6) (2001) A71, http://dx.doi.org/10.1149/1.1368736.

[4] S.S. Zhang, K. Xu, T.R. Jow, The low temperature performance of Li-ion batteries, J. Power Sources 115 (1) (2003) 137–140, http://dx.doi.org/10.1016/S0378-7753(02)00618-3, URL https://www.sciencedirect.com/science/article/pii/S0378775302006183.

[5] Q. Wang, B. Jiang, B. Li, Y. Yan, A critical review of thermal management models and solutions of lithium-ion batteries for the development of pure electric vehicles, Renew. Sustain. Energy Rev. 64 (2016) 106–128, http://dx.doi.org/10.1016/j.rser.2016.05.033, URL https://www.sciencedirect.com/science/article/pii/S1364032116301435.

[6] G. Nagasubramanian, Electrical characteristics of 18650 Li-ion cells at low temperatures, J. Appl. Electrochem. 31 (1) (2001) 99–104, http://dx.doi.org/10.1023/A:1004113825283, URL https://link.springer.com/article/10.1023/A:1004113825283.

[7] J. Fan, S. Tan, Studies on charging lithium-ion cells at low temperatures, J. Electrochem. Soc. 153 (6) (2006) A1081, http://dx.doi.org/10.1149/1.2190029.

[8] T.M. Bandhauer, S. Garimella, T.F. Fuller, A critical review of thermal issues in lithium-ion batteries, J. Electrochem. Soc. 158 (3) (2011) R1, http://dx.doi.org/10.1149/1.3515880.

[9] M. Petzl, M. Kasper, M. Danzer, Lithium plating in a commercial lithium-ion battery–a low-temperature aging study, J. Power Sources 275 (2015) 799–807, http://dx.doi.org/10.1016/j.jpowsour.2014.11.065, URL https://www.sciencedirect.com/science/article/pii/S0378775314018928.

[10] M.C. Smart, B.V. Ratnakumar, S. Surampudi, Electrolytes for low-temperature lithium batteries based on ternary mixtures of aliphatic carbonates, J. Electrochem. Soc. 146 (2) (1999) 486, http://dx.doi.org/10.1149/1.1391633.

[11] E.J. Plichta, W.K. Behl, A low-temperature electrolyte for lithium and lithium-ion batteries, J. Power Sources 88 (2) (2000) 192–196, http://dx.doi.org/10.1016/S0378-7753(00)00367-0, URL https://www.sciencedirect.com/science/article/pii/S0378775300003670.

[12] C.K. Huang, J.S. Sakamoto, J. Wolfenstine, S. Surampudi, The limits of low-temperature performance of Li-ion cells, J. Electrochem. Soc. 147 (8) (2000) 2893, http://dx.doi.org/10.1149/1.1393622.

[13] C. Wang, A.J. Appleby, F.E. Little, Low-temperature characterization of lithium-ion carbon anodes via microperturbation measurement, J. Electrochem. Soc. 149 (6) (2002) A754, http://dx.doi.org/10.1149/1.1474427.

[14] N. Shidore, T. Bohn, Evaluation of Cold Temperature Performance of the JCS-VL41M PHEV Battery Using Battery HIL, SAE Technical Paper, 2008, http://dx.doi.org/10.4271/2008-01-1333.

[15] X. Li, C. Yuan, C. Wang, Multi-time-scale framework for prognostic health condition of lithium battery using modified Gaussian process regression and nonlinear regression, J. Power Sources 467 (2020) 228358, http://dx.doi.org/10.1016/j.jpowsour.2020.228358, URL https://www.sciencedirect.com/science/article/pii/S0378775320306625.

[16] J.A. Lustbader, J.P. Rugh, E.V. Titov, J. Meyer, N. Agathocleous, A. Vespa, Range Extension Opportunities While Heating a Battery Electric Vehicle, SAE Technical Paper, 2018, http://dx.doi.org/10.4271/2018-01-0066, URL https://saemobilus.sae.org/content/2018-01-0066/.

[17] E. Samadani, S. Farhad, S. Panchal, R. Fraser, M. Fowler, Modeling and Evaluation of Li-Ion Battery Performance Based on the Electric Vehicle Field Tests, Vol. 1848, SAE Technical Paper, 2014, pp. 8–16, http://dx.doi.org/10.4271/2014-01-1848.

[18] S. Chowdhury, L. Leitzel, M. Zima, M. Santacesaria, G. Titov, J. Lustbader, J. Rugh, J. Winkler, A. Khawaja, M. Govindarajalu, Total Thermal Management of Battery Electric Vehicles, SAE Technical Paper Series, BEVs, 2018, http://dx.doi.org/10.4271/2018-37-0026, URL https://www.osti.gov/biblio/1461757.

[19] S. Panchal, S. Mathewson, R. Fraser, R. Culham, M. Fowler, Experimental Measurements of Thermal Characteristics of LiFePO 4 Battery, Vol. 1189, SAE Technical Paper, 2015, http://dx.doi.org/10.4271/2015-01-1189.

[20] X. Li, C. Yuan, C. Wang, J. Xie, A data-fusion framework for lithium battery health condition estimation based on differential thermal voltammetry, Energy 239 (2022) 122206, http://dx.doi.org/10.1016/j.energy.2021.122206, URL https://www.sciencedirect.com/science/article/pii/S0360544221024543.

[21] S. Panchal, M. Rashid, F. Long, M. Mathew, R. Fraser, M. Fowler, Degradation Testing and Modeling of 200 Ah LiFePO 4 Battery, Vol. 0441, SAE Technical Paper, 2018, http://dx.doi.org/10.4271/2018-01-0441.

[22] J. Taggart, Ambient temperature impacts on real-world electric vehicle efficiency & range, in: 2017 IEEE Transportation Electrification Conference and Expo, ITEC, IEEE, 2017, pp. 186–190, http://dx.doi.org/10.1109/ITEC.2017.7993269, URL https://ieeexplore.ieee.org/document/7993269.

[23] M. Steinstraeter, T. Heinrich, M. Lienkamp, Effect of low temperature on electric vehicle range, World Electr. Veh. J. 12 (3) (2021) 115, http://dx.doi.org/10.3390/wevj12030115, URL https://www.mdpi.com/2032-6653/12/3/115.

[24] A. Vlahinos, A.A. Pesaran, Energy Efficient Battery Heating in Cold Climates, SAE Technical Paper, SAE Technical Paper, 2002, pp. 826–833, http://dx.doi.org/10.4271/2002-01-1975.

[25] A.A. Pesaran, A. Vlahinos, T. Stuart, Cooling and preheating of batteries in hybrid electric vehicles, in: 6th ASME-JSME Thermal Engineering Joint Conference, Citeseer, 2003, pp. 1–7, URL http://www.aes.nu/publications/2003-CoolingPreheating-JSME.pdf.

[26] Y. Ji, C.Y. Wang, Heating strategies for li-ion batteries operated from subzero temperatures, Electrochim. Acta 107 (2013) 664–674, http://dx.doi.org/10.1016/j.electacta.2013.03.147, URL https://www.sciencedirect.com/science/article/pii/S0013468613005707.

[27] Z. Lei, Y. Zhang, X. Lei, Improving temperature uniformity of a lithium-ion battery by intermittent heating method in cold climate, Int. J. Heat Mass Transfer 121 (2018) 275–281, http://dx.doi.org/10.1016/j.ijheatmasstransfer.2017.12.159, URL https://www.sciencedirect.com/science/article/pii/S0017931017341996.

[28] Z.G. Qu, Z.Y. Jiang, Q. Wang, Experimental study on pulse self–heating of lithium–ion battery at low temperature, Int. J. Heat Mass Transfer 135 (2019) 696–705, 10.1016/j.ijheatmasstransfer.2019.02.020 URL https://www.sciencedirect.com/science/article/pii/S0017931018352803.

[29] J. Jeffs, A. McGordon, A. Picarelli, S. Robinson, W.D. Widanage, System level heat pump model for investigations into thermal management of electric vehicles at low temperatures, in: Proceedings of the 13th International Modelica Conference, Regensburg, Germany, March 4–6, 2019, (157) Linköping University Electronic Press, 2019, http://dx.doi.org/10.3384/ecp19157107, URL https://ep.liu.se/en/conference-article.aspx?series=&issue=157&Article_No=11.

[30] Y. Higuchi, H. Kobayashi, Z. Shan, M. Kuwahara, Y. Endo, Y. Nakajima, Efficient Heat Pump System for PHEV/BEV, SAE Technical Paper, 2017, http://dx.doi.org/10.4271/2017-01-0188.

[31] A. Hande, T.A. Stuart, AC heating for EV/HEV batteries, in: Power Electronics in Transportation, 2002, IEEE, 2002, pp. 119–124, http://dx.doi.org/10.1109/PET.2002.1185559, URL https://ieeexplore.ieee.org/document/1185559.

[32] T.A. Stuart, A. Hande, HEV battery heating using AC currents, J. Power Sources 129 (2) (2004) 368–378, http://dx.doi.org/10.1016/j.jpowsour.2003.10.014, URL https://www.sciencedirect.com/science/article/pii/S0378775303011352.

[33] J. Zhu, Z. Sun, X. Wei, H. Dai, An alternating current heating method for lithium-ion batteries from subzero temperatures, Int. J. Energy Res. 40 (13) (2016) 1869–1883, http://dx.doi.org/10.1002/er.3576.

[34] X. Hu, Y. Zheng, D.A. Howey, H. Perez, A. Foley, M. Pecht, Battery warm-up methodologies at subzero temperatures for automotive applications: Recent advances and perspectives, Prog. Energy Combust. Sci. 77 (2020) 100806, http://dx.doi.org/10.1016/j.pecs.2019.100806, URL https://www.sciencedirect.com/science/article/pii/S0360128519301169.

[35] D. Ouyang, Y. He, J. Weng, J. Liu, M. Chen, J. Wang, Influence of low temperature conditions on lithium-ion batteries and the application of an insulation material, RSC Adv. 9 (16) (2019) 9053–9066, http://dx.doi.org/10.1039/C9RA00490D, URL https://pubs.rsc.org/en/content/articlehtml/2019/ra/c9ra00490d.

[36] Z. Ling, X. Wen, Z. Zhang, X. Fang, T. Xu, Warming-up effects of phase change materials on lithium-ion batteries operated at low temperatures, Energy Technol. 4 (9) (2016) 1071–1076, http://dx.doi.org/10.1002/ente.201600083.

[37] H. Wu, X. Zhang, C. Wang, R. Cao, C. Yang, Experimental study on aerogel passive thermal control method for cylindrical lithium-ion batteries at low temperature, Appl. Therm. Eng. 169 (2020) 114946, http://dx.doi.org/10.1016/j.applthermaleng.2020.114946, URL https://www.sciencedirect.com/science/article/pii/S135943111933234X.

[38] Gamma Technologies Inc, GT-suite user manual, 2020.
[39] A. Ramesh Babu, J. Andric, B. Minovski, S. Sebben, System-level modeling and thermal simulations of large battery packs for electric trucks, Energies 14 (16) (2021) 4796, http://dx.doi.org/10.3390/en14164796, URL https://www.mdpi.com/1996-1073/14/16/4796.
[40] T.H. Chilton, A.P. Colburn, Mass transfer (absorption) coefficients prediction from data on heat transfer and fluid friction, Ind. Eng. Chem. 26 (11) (1934) 1183–1187, http://dx.doi.org/10.1021/ie50299a012.
[41] T. Huria, M. Ceraolo, J. Gazzarri, R. Jackey, High fidelity electrical model with thermal dependence for characterization and simulation of high power lithium battery cells, in: 2012 IEEE International Electric Vehicle Conference, 2012, pp. 1–8, http://dx.doi.org/10.1109/IEVC.2012.6183271.
[42] D. Bernardi, E. Pawlikowski, J. Newman, A general energy balance for battery systems, J. Electrochem. Soc. 132 (1) (1985) 5, http://dx.doi.org/10.1149/1.2113792.
[43] Q. Sun, H. Zhang, J. Zhang, W. Ma, Adaptive unscented kalman filter with correntropy loss for robust state of charge estimation of lithium-ion battery, Energies 11 (11) (2018) 3123, http://dx.doi.org/10.3390/en11113123, URL https://www.mdpi.com/1996-1073/11/11/3123.
[44] J.A. Nelder, R. Mead, A simplex method for function minimization, Comput. J. 7 (4) (1965) 308–313, http://dx.doi.org/10.1093/comjnl/7.4.308.
[45] A. Pesaran, S. Santhanagopalan, G.H. Kim, Addressing the Impact of Temperature Extremes on Large Format Li-Ion Batteries for Vehicle Applications (Presentation), Technical Report, National Renewable Energy Lab.(NREL), Golden, CO (United States), 2013, URL https://digital.library.unt.edu/ark:/67531/metadc834057/m1/1/.
[46] P.R. Tete, M.M. Gupta, S.S. Joshi, Developments in battery thermal management systems for electric vehicles: A technical review, J. Energy Storage 35 (2021) 102255, http://dx.doi.org/10.1016/j.est.2021.102255, URL https://www.sciencedirect.com/science/article/pii/S2352152X21000232.
[47] T.J. Barlow, S. Latham, I.S. McCrae, P.G. Boulter, A Reference Book of Driving Cycles for Use in the Measurement of Road Vehicle Emissions, TRL Published Project Report, 2009, URL https://trid.trb.org/view/909274.
[48] Thermal insulation materials, technical characteristics and selection criteria, 2022, https://www.fao.org/3/y5013e/y5013e08.htm. (Accessed 11 March 2022).
[49] E. Mattarelli, A. Muscio, Potential of thermal engine encapsulation on automotive diesel engines, in: 7th International Conference on Engines for Automobile, ICE 2005, Vol. 2005, SAE International, 2005, http://dx.doi.org/10.4271/2005-24-067.